Direct Measurement of the Direction, Size and Velocity of Droplets Generated by Top-blowing

Tim Haas, Aron Ringel, Ville-Valtteri Visuri, Moritz Eickhoff and Herbert Pfeifer*

Tim Haas, Aron Ringel, Moritz Eickhoff, Prof. Dr. Herbert Pfeifer
Department for Industrial Furnaces and Heat Engineering, RWTH Aachen University, Kopernikusstraße 10, D-52074 Aachen, Germany
E-mail: haas@iob.rwth-aachen.de

Dr. Ville-Valtteri Visuri
Process Metallurgy Research Unit, University of Oulu, PO Box 4300, FI-90014 University of Oulu, Finland

Keywords: Droplet diameter, droplet velocity, splashing angle, top-blowing, image processing

Abstract: Problems associated with top-blowing are present in most steel plants. While it promotes high reaction rates, it can cause loss of yield, working hazards and increased maintenance cost by spitting, skulling or lid sticking. Although the basic physics of the splashing phenomenon have already been established, earlier studies have not addressed the velocities of splashing droplets. Furthermore, existing information on the size and impingement angle of the droplets is based on indirect measurements. In this work, a direct measurement method for splashing droplets is developed that obtain the number of droplets, the splashing angle, the droplet velocity and diameter simultaneously. It is found that existing correlations overestimate the droplet diameter because they are biased by the indirect method and overfit results obtained with raw iron. Grid measurements indicate that all droplet properties strongly depend upon the sampling position. Finally, the splashing angle was found to become steeper while the lance height decrease. However, the effect is less correlated with the cavity mode than assumed in the literature. Further measurements are proposed, using the methodology developed in this work, to derive more comprehensive droplet property correlations. By that, lance designs and blowing practices can be optimized.

1. Introduction

The basic oxygen furnace (BOF) process and the argon oxygen decarburization (AOD) are the most common processes for the refining of steel and stainless steel, respectively. Both account for over 70% of the annual production in their sectors. The processes are characterized by high metallurgical reaction rates that are achieved by an extensive mixing and by equipping the vessel with an oxygen top lance. Typically, the top lance is fitted with a de Laval nozzle, which produces a supersonic jet that impinges on the melt with a high momentum, penetrates the surface and forms a cavity, while extensively oxidizing impurities, iron and alloying elements. Inside the cavity, the jet is redirected, causing high shear forces at the surface. In case the shear force outweighs the restoring surface tension and inertia forces, liquid sheets constrict and form dispersed metal or slag droplets that impinge with a high momentum[1]. The droplets collide with the furnace lining and shorten the lifetime of the refractory above the bath level. By this, the refractory costs are significantly increased while the operational time of the furnace is reduced. A crucial problem are splashing droplets in processes where the lid of the vessel can be moved. They can cause a sticking of the lid and long standstills. In case the droplets are impinged out of the converter mouth, the phenomenon is known as spitting, causing working hazards and yield loss. Another significant problem arises from skulling, which is caused by droplets that attach on the lance itself.

In order to overcome these problems, experimental as well as numerical studies were carried out. The most comprehensive studies have been published by Koria and Lange[2-4] in lab-scale experiments with liquid metal and by Brooks and coworkers[5-11] based on physical and numerical studies. Koria and Lange[3] proposed a dimensionless momentum number, which can be used to estimate the cavity depth, cavity diameter, droplet generation rate and droplet size:

$$N_{Mo} = \frac{0.7854 \cdot 10^5 d_n^2 N p_a \left(1.27\frac{p_a}{p_0} - 1\right)}{\rho_l g H^3} \quad (1)$$

where d_n is the nozzle diameter, N is the number of nozzles, p_a is the ambient pressure (given in unit bar), p_0 is the supply pressure (in bar), ρ_l is the liquid density and H is the lance height. Koria and Lange[3] indirectly measured the droplet size in a lab-scale experiment by analyzing all raw iron droplets that fell out of the crucible on a sampling sheet. They proposed a Rosin-Rammler-Sperling (RRS) distribution to describe the resulting range of droplet diameters:

$$Y(d) = 100 \cdot exp\left[-\left(\frac{d}{d'}\right)^n\right] \quad (2)$$

where Y(d) denotes the cumulative weight-percentage of droplets larger than d, d' is a measure of fineness that is defined as the diameter larger than the smallest 36.8 % of droplets, n is a distribution parameter in the range of 1 to 1.828. For raw iron they proposed a n value of 1.26. For the measure of fineness d' they proposed[4]:

$$d' = \left(\frac{3}{\log(e)}\right)^{-\frac{1}{n}} \cdot 5.513 \cdot 10^{-6} \cdot \left[10 \cdot \frac{d_n^2}{H^2} \cdot p_a \left(1.27\frac{p_0}{p_a} - 1\right) cos(\theta)\right]^{1.206} \quad (3)$$

where θ denotes the nozzle inclination angle and p_a is given in unit bar.

In addition, Ji *et al.*[12] showed in a subsequent study that d' is a function of the sampling position. A benefit of the correlations derived by Koria and Lange is that all parameters are directly accessible in a steel plant. A major problem of these correlations is though, that they were derived based on a few measurements and cannot be applied to every vessel.

Based on the works of Block *et al.*[13], He and Standish[14], Li and Harris[15] and own measurements, Subagyo *et al.*[5] proposed the more generalized blowing number:

$$N_B = \frac{\rho_g u_t^2}{2\sqrt{\sigma g \rho_l}} \quad (4)$$

where ρ_g is the density of the gas jet, u_t is the tangential velocity of the gas jet at the impingement zone, σ is the surface tension of the liquid and ρ_l is the density of the liquid. The

tangential velocity at the impingement zone can be estimated by the empirical correlation by Deo and Boom[16] and Li and Harris[15]:

$$u_t = \eta u_i \quad (5)$$

where η is a constant with the value 0.4472 for straight nozzles and u_i is the axial velocity of the jet. The blowing number can be used to predict the onset of splashing, the droplet rate and the droplet diameter. The droplet diameter was measured by analyzing droplets that stick to the lid of the vessel[5]. Droplet diameters between 0.3 to 90 mm were measured with a Sauter mean diameter of 9.5 to 21 mm. Combining their data with the existing data of Koria and Lange[4, 17], a Rosin-Rammler-Sperling distribution was proposed where d' can be estimated by:

$$d' = 12.0 \cdot (N_B)^{0.82} \quad (6)$$

It was reported that, while the limiting droplet diameter strongly depend upon the blowing number, the spreading parameter n was almost independent of it. In comparison to the momentum number, the blowing number has the advantage that it is based on the physical background of the Kelvin-Helmholtz-Instability. As discussed in the literature[9, 18], the original form of the blowing number theory proposed by Subagyo *et al*.[5] does not scale properly to conditions in a real converter. Consequently, later studies have suggested modifications to enable better upscaling. Alam *et al*.[8] suggested that the value of η depends on the inclination angle of the gas jets, while Sabah *et al*.[9] found that η is constant only for a given cavity mode. Rout *et al*.[11] suggested that the gas flow rate used for calculating the droplet generation rate should be scaled to conditions of the bath surface. Despite its shortcomings the blowing number theory has been employed in reaction models for different metallurgical processes involving top-blowing[19-21].

There are multiple other studies aiming at a general physical understanding of splashing[18, 22-25]. For instance, it has been found that combined-blowing increases the droplet generation rate significantly[26, 27], while a slag layer decreases it[27].

Another important work was carried out by Molloy[28] who defined three different cavity modes, namely the dimpling, the splashing and the penetrating mode which are characterized by different cavity shapes, cavity oscillations and splashing behaviors. In dimpling mode, the gas jet disturbs the bath surface weakly. Its role in industrial applications is negligible. By exceeding a critical cavity depth, the splashing mode becomes active. The shear force is sufficiently high to create droplets that impinge mainly radially outwards of the cavity. A further increment of the momentum causes a deeper cavity. In the penetration mode, generated droplets remain in the cavity or they are hurled upwards rather than sideward. Owing to that, the overall droplet generation rate is decreased[26].

The aforementioned studies have created a fundamental basis for the understanding of the splashing phenomenon as well as for an improvement of the blowing practice. However, there are also some limitations, such as the fact that the droplet size and the splashing angle were only measured indirectly and correlations are based on very few experiments. The droplet velocity has not yet been measured. However, an understanding of these quantities is crucial for reaction models and the improvement of the top lance design. Thus, direct measurement of the droplet diameter, velocity and splashing angle are made in this work. Preliminary measurements of the gas jet velocity and the cavity depth are made to correlate the results with both, the lance height as well as the blowing number.

2. Experimental setup

In three different experiments, the gas jet momentum, the cavity depth and the number, size, velocity and direction of the impinging droplets are determined. The first two measurements are important to derive the dimensionless blowing number. By that, the droplet properties can be compared with literature data.

2.1 Jet momentum

The jet momentum for different lance pressures and at different positions along the axial direction is obtained by measuring the jets dynamic pressure with a pitot tube. For that, the lance is attached to a rail underneath which a pitot tube is placed. For gauge pressures of 0.5 bar and 1 bar, the height is shifted from 5 cm to 40 cm by increments of 5 cm towards the pitot tube. Taking the pressure dependency of the density into account, the axial gas velocity u_i was calculated by:

$$u_i = \sqrt{\frac{2p_{dyn}}{p_a + p_{dyn}} R_L T} \quad (7)$$

where p_{dyn} is the dynamic pressure in Pa, R_L is the specific gas constant of air and T is the temperature.

The cavity depth and splashing experiments are carried out in an acrylic glass cuboid, filled with tap water. The dimensions of the tank are 300 x 300 x 250 mm and the filling height is 220 mm. Above the center of the tank, a lance is placed. The lance orifice has a diameter of 3.6 mm. A pressure regulator allows controlling and varying the lance pressure.

2.2 Cavity depth

To measure the cavity depth, a camera (Canon EOS 5DS, resolution: 50.6 megapixels) is placed such that it records the cavity depth from the side. The cavity depth is measured manually using the MATLAB imaging toolbox. For each setting, fifty images are used to calculate the time-averaged depth of the oscillating cavity.

2.3 Droplet property measurements

2.3.1. Setup

The droplet size, velocity, direction and number are evaluated simultaneously by digital image processing. Since the droplets are very small and fast, the measurement setup comprises a double frame camera (LaVision Imager Pro X 4M), a mounted microscope lens and a high intensity backlight diffusor. The measurement setup can be seen in **Figure 1**. The

diffusor produces a homogenous backlight that simplify the subsequent image processing. The backlighting is pulsed synchronous with the camera, so that no frame of a double frame is overexposed. The camera's resolution is 2048 x 2048 pixels and the delay time between two frames is 400 µs. The microscope lens narrows the focal plane to an area of about 15 x 15 mm. By that, droplets on a micrometer scale can be detected with a high resolution. The size of the focal area is a tradeoff between the ability to detect small or large droplets. In case the focal area is too large, small droplets and image noise are difficult to distinguish. In case it is too small, large droplets do not fit on the image and cannot be detected. However, by a visual verification, no frame could be found that was covered by a single droplet by more than 50 percent. The position of the focal area is chosen in a way so that the velocity component perpendicular to the camera is negligible. Another novelty of this study is that the measurement quantities are not only obtained at a fixed position, but on a measurement plane. For that, the camera and the diffusor were shifted so that a measurement grid was covered. The vertical position was varied in increments of 15.5 mm from 86.5 mm to 164.0 mm, there the jet axis was defined as the point of origin. The horizontal position was varied from 7.0 mm to 177.5 mm in 15.5 mm steps there the bath surface was defined as the point of origin. Four different lance heights of 50 mm, 100 mm, 200 mm and 300 mm were investigated with a lance gauge pressure of 1 bar. For the droplet analysis it was assumed that the splashing profile has an axial symmetry. This assumption is more appropriate in case of longer sampling. Thus, for each combination of lance height and measurement position, 50 double frames were taken with a recording rate of 5 Hz.

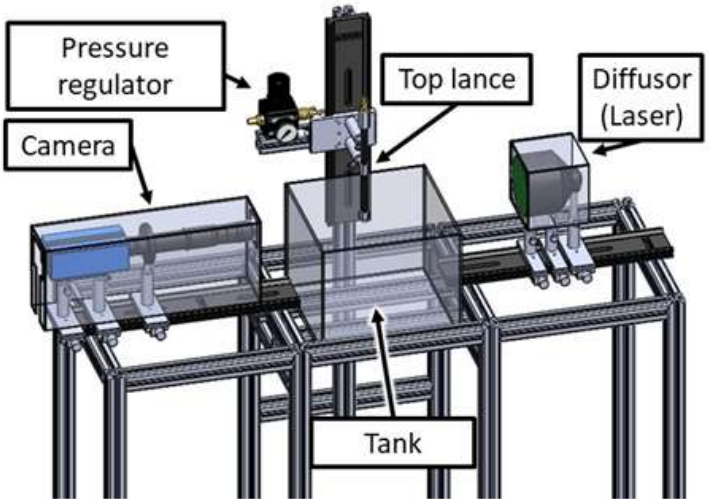

Figure 1: Experimental setup

2.3.1. Image processing

An image processing procedure is developed to derive the droplet quantities from the double frames. It needs to solve two different challenges. First, it has to identify individual droplets as objects on both frames. Subsequently, a droplet detected on the first frame need to be assigned to the same droplet found on the second frame. Only those droplets detected in both frames are considered for statistical analysis.

A representative frame is shown in Figure 2 a. For detection, all double frames are preprocessed by Wiener filter to reduce the impact of image noise. Then, gradients in the grayscale level of the frames are computed by applying a Sobel filter:

$$G_x = \begin{bmatrix} 1 & 0 & -1 \\ 2 & 0 & -2 \\ 1 & 0 & -1 \end{bmatrix} \circ F \quad G_y = \begin{bmatrix} 1 & 2 & 1 \\ 0 & 0 & 0 \\ -1 & -2 & -1 \end{bmatrix} \circ F \tag{8}$$

where ° denotes a convolution operation, G_x and G_y represents the grayscale gradient in x, respectively in y-direction and F is the receptive field. The receptive field is a matrix of the same dimension than the filter that contains the gray level of the pixel of the image for that the gradient is computed and all neighboring ones. It is slide through all rows and columns of the image so that the gradient is computed for every pixel. The gradient magnitude is computed by:

$$G = \sqrt{G_x^2 + G_y^2} \quad (9)$$

The result of the Sobel operation can be seen in Figure 2 b. After computing the gradients, thresholding is applied to binarize the image (Figure 2 c). Those gradients that exceed this threshold are kept and assigned to a positive. In case objects are too far from the focal plane, its outlines appear blurry and its gradients are below the threshold. Objects that are only partially in the frame are not further considered to avoid distortion of the diameter estimation. In addition, strong gradients extending over a small area are considered image noise and are not processed further. Finally, an object detection algorithm is applied that identify clusters of connected positive pixels in the binarized image, shown in Figure 2 d.

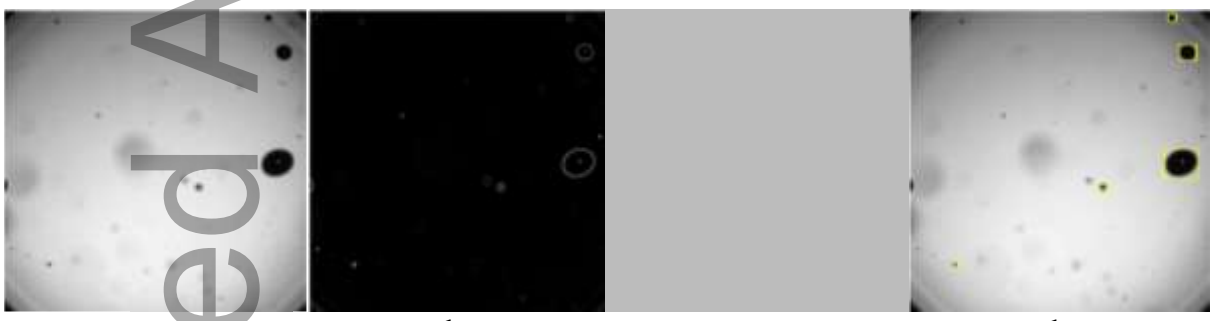

a b c d

Figure 2: Steps of image processing: a)original image b) Sobel filtering c) thresholding d) object detection

The second task of the image processing procedure is to identify detected objects which are visible in both frames. These objects are combined to one track. The assignment is made by computing an empirical cost function J for all possible combinations of detected objects in a double frame:

$$J = \frac{\sqrt{(x_{F1} - x_{F2})^2 + (y_{F1} - y_{F2})^2}}{5} + \frac{3 \cdot \max(d_{F1}, d_{F2})}{\min(d_{F1}, d_{F2})} \quad (10)$$

where x and y are the coordinates of an object and d is its diameter while F1 and F2 denotes the frame in which the object is in. The pair that yield the lowest cost function is assigned to each other and considered as the same droplet found in subsequent frames.

In case all cost functions are above a specified threshold, the detection remains unassigned and is not further considered. For assigned droplets, the diameter is computed by:

$$d = \frac{d_{\max,F1}+d_{\min,F1}+d_{\max,F2}+d_{\min,F2}}{4} \circ C_{\text{spatial}} \quad (11)$$

where C_{spatial} is the conversion factor between pixels and meter that is obtained from a calibration image. The droplet velocity is obtained from the shift of the droplets center multiplied by the spatial and temporal scale factor. The splashing direction is the angle between the velocity vector w and the positive x-axis computed by:

$$\cos(\theta) = \frac{w \cdot x}{|w| \cdot |x|} \quad (12)$$

Since only those droplets that are completely visible in both frames are taken into account, smaller and slower droplets are more likely be detected that larger or faster ones. The detection probability as a function of size and velocity is shown in **Figure 3**. The detection probabilities are based on synthetically generated spherical droplets. For the computation of average droplet velocity and diameter, these probabilities are taken into account as described later.

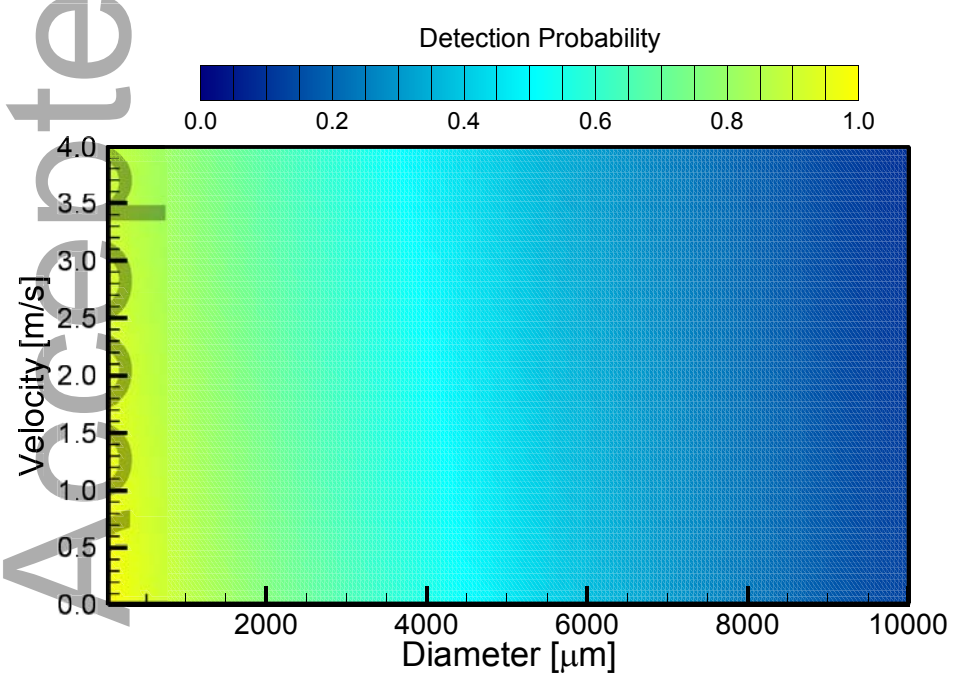

Figure 3: Detection probability as a function of droplet diameter and velocity

To enable comparison with the observations by Subagyo *et al.*[5] and Koria and Lange[4], the Sauter mean diameter was computed by:

$$d_{32} = \frac{\sum_{i=1}^{n} n_i d_i^3}{\sum_{i=1}^{n} n_i d_i^2}. \quad (13)$$

3. Results

A characteristic scatter plot of all detected droplets for a lance height of 100 mm is shown in **Figure 4**. It can be seen that most detected droplets are in a diameter range between 0 and 3000 µm. For those droplet diameters, the droplet velocity is distributed between 0 and 9 m s^{-1}, though most droplets velocities are in the range of 0 to 4 m s^{-1}. Larger droplets were only detected in case their velocity was low. However, considering the detection probabilities, it is likely that some large and fast droplets exist that could not have been detected in both frames. Thus, they are not further processed and are not shown in the scatterplot. To take account for that bias, the detection probability is used to compute adjusted means. In the subsequent analysis, this is made by sorting all detections to a finite number of diameter and velocity ranges. The adjusted number and diameter are computed by dividing the number of droplets in each range by the detection probability for the range shown in Figure 3. The number of droplets in each range is thereafter divided by the detection probability for that range that is shown in Figure 3. With that adjusted number, the adjusted diameter, respectively velocity, is computed.

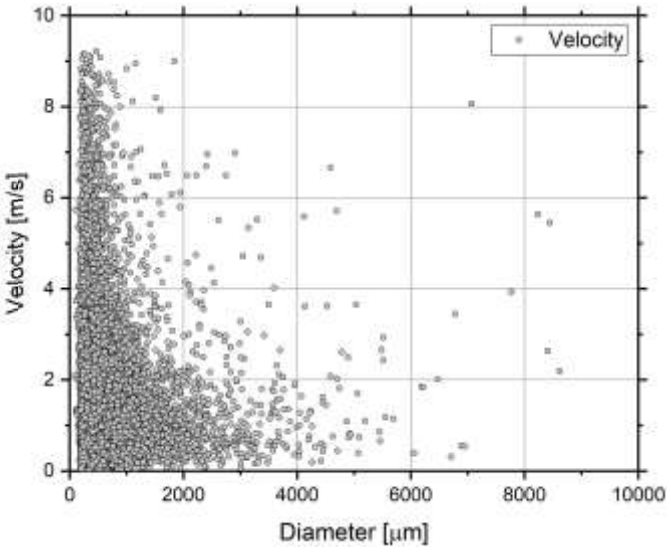

Figure 4: Scatter plot of all detected droplets for a lance height of 100 mm (N_B=5.92)

3.1 Averaged data

The total number of detected droplets in dependence of the lance height is given in **Figure 5**. In addition, the according blowing numbers are given. The blowing numbers are based on the preliminary measurements of the cavity depth and the gas jet velocity and are computed using **Equation 4** and **5**. In case of a high lance height, the number of detections is very low. It increases in case the lance height is lowered to 200 mm, respectively 100 mm. The slope seems to follow linear patterns though the number of data points is too low for a valid conclusion. A further decrease of the lance height reduces the number of detections significantly. This phenomenon is probably attributed to the change of cavity mode.

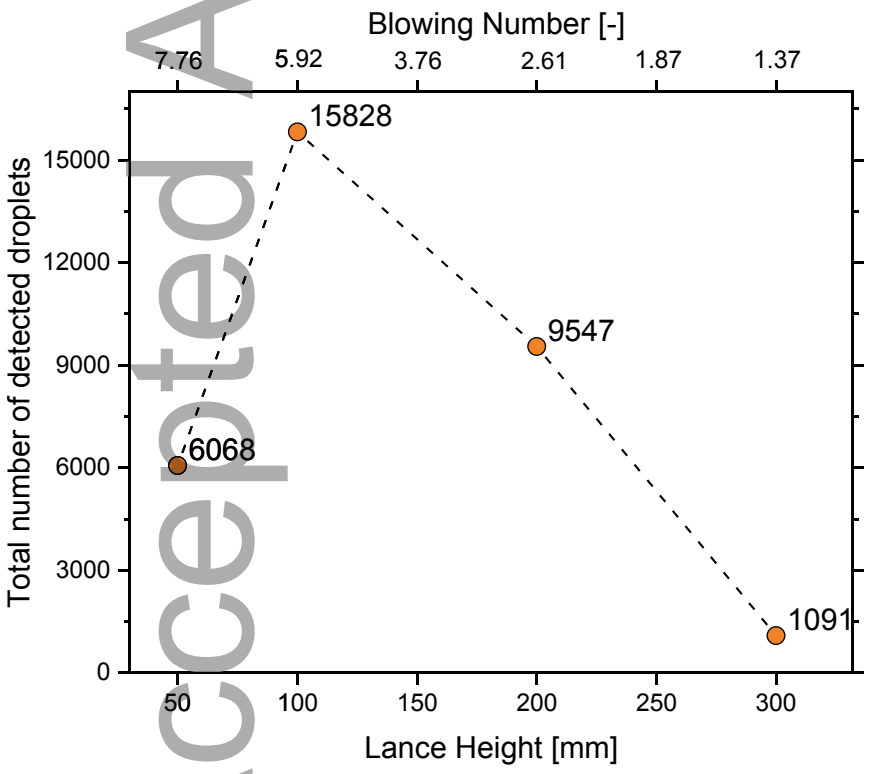

Figure 5: Dependence of the number of droplets on the lance height and the blowing number, respectively

In **Figure 6**, the droplet diameter is shown for different lance heights, blowing numbers respectively, as a boxplot. The average mean value is given by diamond shaped markers, connected with a dotted line. To take account for the measurement bias, the average mean value is computed considering the detection probabilities. Its values are highlighted by a

white background. For a better comparison with the observations by Subagyo *et al.* [5], the Sauter mean diameter is also computed using **Equation 13**. The values are shown by a star-shaped marker. Again, its value is given, highlighted by underlining it. Like for the mean diameter, the values consider the detection probabilities. The experiments indicate that both average droplet diameters increase while the lance height decrease, respectively the blowing number increase. In addition, the maximum diameter as well as the diameter range were found to increase.

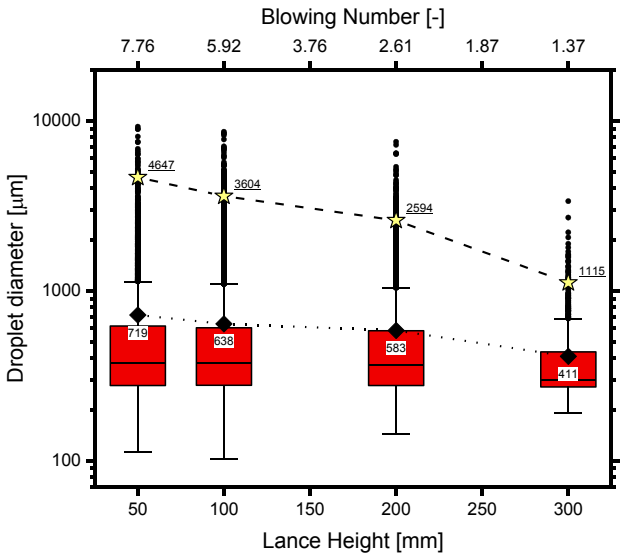

Figure 6: Boxplot of detected droplet diameters for different lance heights, including the average mean (diamond-shaped) and Sauter mean (star-shaped) diameter.

The different droplet diameter distributions, adjusted by considering the detection probabilities, were correlated with the Rosin-Rammler distribution (**Equation 2**). The distribution parameters and their correlation values are summarized in **Table 1**. In addition, the theoretical values computed with **Equation 3** and **6** are given. It can be seen that both correlations significantly overestimate the droplet diameter for the given conditions. The effect is most pronounced for the correlation of Subagyo *et al.* [5] for a low lance height. Furthermore, it can be seen that the distribution parameter n is not constant as reported by Subagyo *et al.*[5]. In contrast, it shows a strong dependency on the blowing number, the lance height respectively. This indicates that the existing equations overfit the results obtained in experiments made with raw iron and that they are inaccurate in case they are applied to

different fluids. This is a particular problem because blowing is applied in different processes and the fluid properties can differ significantly, even in different stages of the same process. Owing to that, a more comprehensive correlation is necessary. However, the number of data points in this work is far too small to derive such an equation that covers the whole complexity of the problem.

Table 1: Measured Rosin-Rammler-Sperling distribution parameters and comparision with literature data

Lance Height	Blowing number	Rosin Rammler parameters			Sugagyo *et al.*[5]	Koria and Lange [4]
H [7]	[-]	d' [µm]	n	R	d'[µm]	d' [µm]
50	7.76	580	1.18	0.98	64400	54500
100	5.92	548	1.33	0.99	51600	12300
200	2.61	520	1.43	0.99	26300	2600
300	1.37	376	2.34	0.99	15500	1600

The measured droplet velocities are shown as boxplots in **Figure** 7. The mean droplet velocities, considering the detection probability, increase very slightly with decreasing lance height in a range from 1.42 m s^{-1} to 1.46 m s^{-1}. However, the velocity decreases significantly in case the lance height is reduced from 100 mm to 50 mm to 1.05 m s^{-1}. Interestingly, this is identical with the change of the cavity mode. The results show that the droplet velocity differs significantly from the tangential velocity of the gas jet computed by Equation 5 that is in a range between 7 and 18 m s^{-1}. In addition, there is no linear relation between those values. Instead, the cavity mode seems to have an important effect on the droplet velocity.

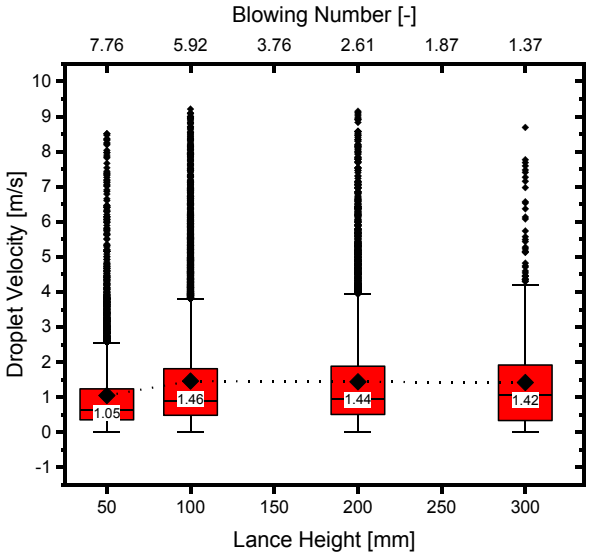

Figure 7: Boxplot of detected droplet velocites for different lance heights, including the average mean (diamond-shaped) diameter

3.2 Grid measurements

Indirect measurements have indicated that the measured droplet quantities might depend upon the sampling position [12]. Thus, direct grid measurements were made in this study to investigate this dependency. For a better visualization, an interpolation between the recorded data points were made. **Figure 8 (a)** to **(d)** show the number of detected droplets in dependency of the lance height and the measurement position. The position of the lance is indicated on the left. In addition, the mean splashing direction is given by vectors. For lance heights of 50 mm and 100 mm, the highest number of detected droplets were found at the sampling positions closest to the lance. The number of detections declines strongly with increasing radial distance to the lance. The vector fields for both lance heights looks similar. On average, the droplet seems to impinge with a steep angle out of the cavity and fall in a relatively small radial distance back into the bath. As was already known from the averaged data, the overall number of detections is significantly higher in case of a lance height of 100 mm.

For a lance height of 200 mm, the maximum number of detected droplets can be found at the lower center of the measurement area. The vector field indicate that the averaged splashing

angle is shallower compared to smaller lance heights. Owing to that, the droplet velocity at the measuring positions furthest away from the lance still have a radial component while it just had a negative axial one in case of smaller lance heights. The number of detections at these positions exceeds those of a lance height of 100 mm, even though the total number of detections in this case in higher by far. For the maximum lance height of 300 mm, the number of detections is small for all sampling positions. The maximum number can be found at the lower right corner of the measurement field, furthest from the lance. This indicates that the averaged splashing angle has become shallower. The vector field do not indicate cohesive mean trajectories in this case. This can be explained by the low numbers of detected droplets at each measurement position. Due to that, the mean angle is clearly distorted by single detections.

The results suggest a relationship between the splashing angle and the blowing number, the lance height respectively. The higher the blowing number, the steeper the mean splashing angle becomes. However, since the first two cases have almost indistinguishable vector fields, it seems that a maximum splashing angle is reached with a lance height of 100 mm. In contrast to existing theories, the maximum is reached before the change of the cavity mode. This indicates that splashing angle and cavity mode are not that strongly correlated than suggested. In addition, the grid measurements showed that measurements of the droplet generation rate depend on the sampling position. It is likely that the droplet generation rate for a lance height of 300 mm is higher than suggested in Figure 5, but that the splashing angle is so shallow that the majority of droplet trajectories are below the measurement plane.

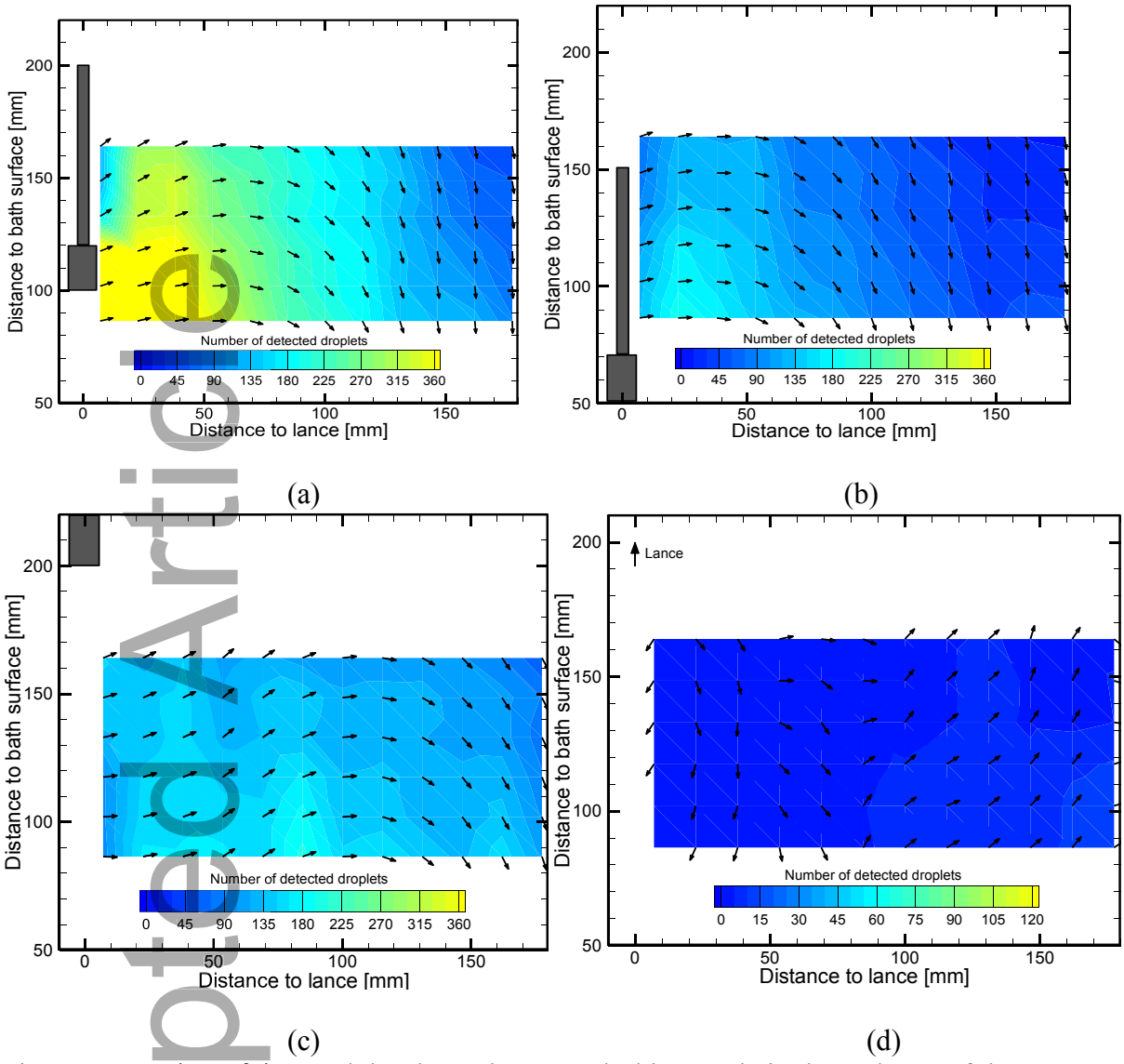

Figure 8: Number of detected droplet and mean splashing angle in dependency of the measurement position for lance heights of (a) 50 mm (N_B=7.76, penetration mode), (b) 100 mm (N_B=5.92, splashing mode), (c) 200 mm (N_B=2.61, splashing mode), and (d) 300 mm (N_B=1.37, splashing mode)

In **Figure 9 a** and **b** the mean droplet diameter and the maximum droplet diameter are shown in dependence of the measurement position for a lance height of 100 mm (N_B=5.92). The mean droplet diameter differs significantly with the sampling position. While it exceeds 650 µm close to the lance, it decreases almost linear to about 450 µm furthest away from the lance. The maximum droplet diameters dependency of the sampling position is less smooth because the value depends on a single droplet. Interestingly, it shows a strong drop from about 5000 to 2000 µm in the upper right corner of the measurement field. The results can be explained by two different phenomena. First is the disintegration of larger droplets into

smaller ones along its trajectories. By that, the number of larger droplets would become smaller with increasing distance to the lance and so would the mean values. This explanation is supported by the measured maximum droplet diameters. Another, less intuitive explanation is that the trajectories of individual droplets depend upon the droplet size. Thus, larger droplets might fall in a radial distance from the lance that exceeds the measurement area. The sampling positions at the distant edge of the area might have a higher likelihood to be crossed my intermediate sized droplets. A further expansion of the measurement grid could prove to what extent both explanations contribute to the observations.

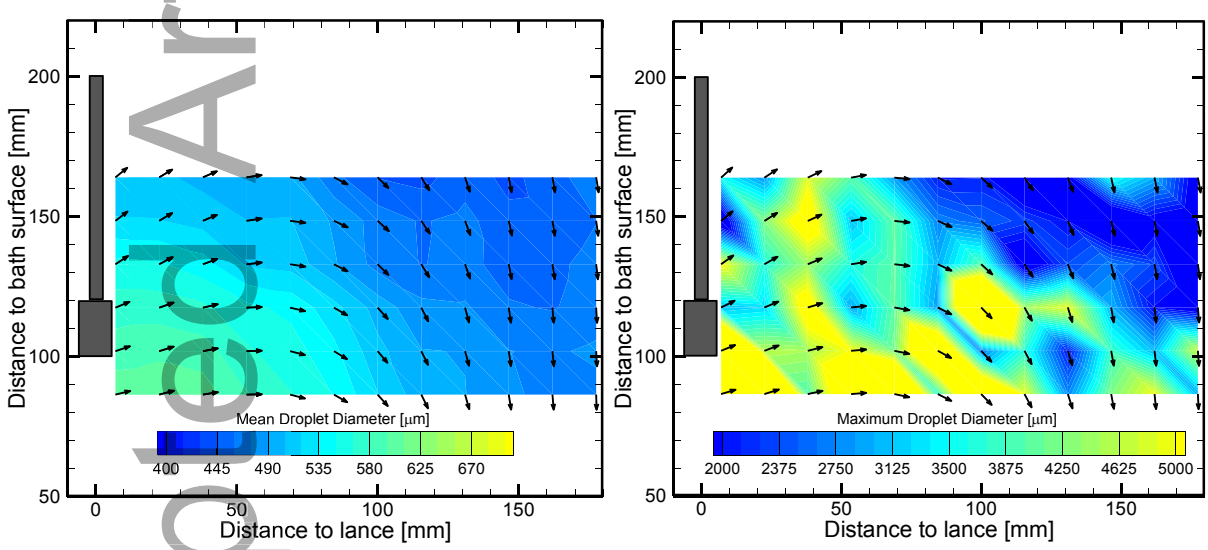

Figure 9: Mean droplet diameter (a) and maximum droplet diameter (b) in dependency of the measurement position for a lance height of 100 mm (N_B=5.92, splashing mode)

The mean droplet velocity in dependency of the sampling position is shown in **Figure 10** for a lance height of 100 mm. Close to the lance, the mean droplet velocity is about 1.9 m s^{-1}. Along the trajectories, the mean velocity gradually declines to a value of about 0.6 m s^{-1} in the lower right corner. The droplet velocity profile matches the mean droplet trajectories very well. It is therefore concluded that the reduction of velocity is due to the decelerating effect of the drag force.

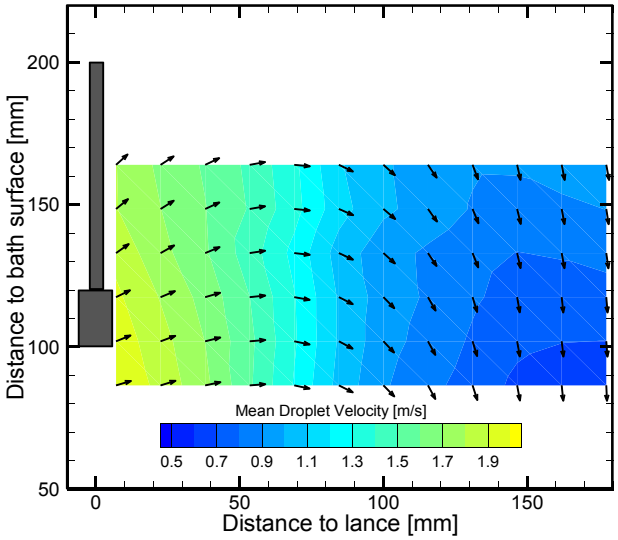

Figure 10: Mean droplet velocity in dependency of the measurement position for a lance height of 100 mm (N_B=5.92, splashing mode)

The grid measurements indicate that all measured quantities strongly depend upon its sampling position. Therefore, realistic averaged quantities can only be obtained if a large measuring grid is covered.

4. Discussion

The efficiency of steel refining in secondary metallurgy processes is often enhanced by equipping the vessel with a top lance. However, accompanied with many benefits, high shear forces in the cavity, caused by the impinging gas jet, induce a splashing of metal or slag droplets. Related problems like spitting, skulling or lid sticking are commonplace in many steel plants. This study was the first to measure droplet quantities directly by imaging. By that, a deepened understanding of the splashing phenomenon was intended.

For direct droplet measurements, an experimental setup comprising of a double frame camera equipped with a microscopic lens was build. This allowed the detection of a broad range of droplet diameters and velocities including very small droplets. Even though the quantities were directly measured, the averaged results were slightly biased by the chosen focal area and the shift between the frames. Both was a compromise between accuracy on the one hand and the maximum detectable value on the other. The bias was partly outbalanced by computing

and considering the detection probabilities of droplets with different diameters and velocities. In addition, the chosen hyperparameters of the subsequent image analysis, for instance the gradient threshold, had a small impact on the results.

For four different lance heights, measurements were conducted at 72 different sampling positions. Thus, the experiments yielded averaged data for the droplet diameter and velocity as well as area measurements that showed the droplet properties in dependency of the measurement position. It has been found that the sampling position had a very large influence on the measured droplet diameter and velocity as well as number of detected droplets and the splashing angle. It is therefore very important that in all further measurements a large range of measurement positions is covered so that the data obtained is not biased by the sampling position. In addition, the area measurement gave quantitative evidence that the splashing angle depend upon the blowing number, the lance height respectively. Interestingly, it was found that the transition from splashing to penetration mode had a smaller impact on the splashing angle than expected. While it was shown that high lance heights resulted in a shallow splashing angle, a lance height of 100 mm, at which the cavity was still in splashing mode, already yielded in a very steep angle. A further decrease of the lance height, that was associated with a change of cavity mode, almost did not change the angle any more. The splashing angle is an important factor for the prediction of droplet trajectories and its understanding is crucial for the improvement of lance head designs. Thus, further studies are proposed including different nozzle inclination angles, different fluid properties and additional lance heights.

The averaged diameter revealed some drawback of existing correlations. In correspondence with Subagyo *et al.*[5], it was found that the averaged droplet diameter increased with increasing blowing number. However, the functional relation seemed to be slightly different from those derived by Subagyo. While the droplet diameter increased with the power of 0.82 in their correlation, the exponent in this work was smaller. Koria and Lange [4] found that the

droplet diameter is related to the lance height by the power of -2.412. In this study, the exponent seemed to be larger, in the range between -0.5 and -1. The most notably difference for all blowing numbers was that the mean droplet diameter was considerably smaller than found by Subagyo *et al.*[5] and Koria and Lange[4]. A possible explanation is a relation between the droplet size and the fluid properties that has not been identified yet. Both studies were made with raw iron, while water was used in this study. Especially the much higher surface tension of steel might be underrepresented in the existing correlations. Some of the deviation can be explained by the indirect measurement method used in the existing studies. Only those droplets were sampled that could be found on a sampling sheet outside the crucible. To illustrate the bias of these studies, the trajectories for different droplet diameters are shown in **Figure 11**. For the calculations, the average droplet velocity (1.8 m s^{-1}) and the average angle (50 degree) at the lower left measurement position for a lance height of 100 mm was used. The drag force was computed by using the drag coefficient correlation derived by Clift *et al.*[29] for rigid, spherical droplets, using the assumption of quiescent air:

$$C_D = \frac{24}{Re_p}(1 + 0.1935 \cdot Re^{0.6305}) \quad (14)$$

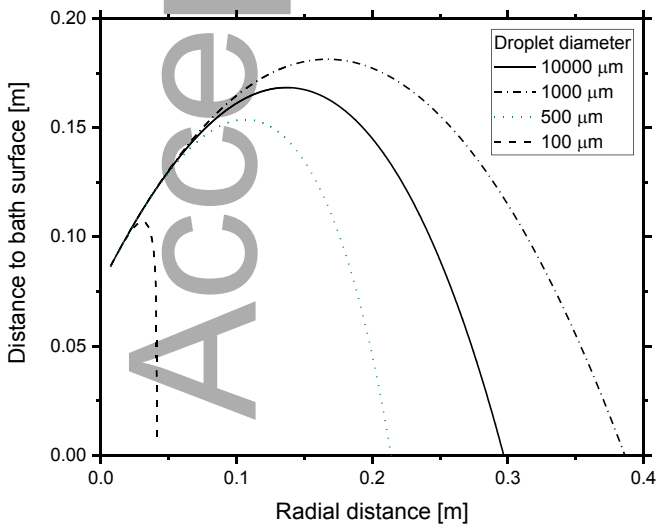

Figure 11: Computed droplet trajectories for different droplet diameters

The computed trajectories show that small droplets fly a small radial distance. Thus, it is likely that most small droplets fell into the crucible rather than being collected on the

sampling sheets. In addition, Figure 11 helps to explain the observations by Ji *et al.*[12] who found that the mean diameter of sampled droplets increased with increasing height of the sampling position. In this work, it was found that the majority of droplets were in a range of a few hundred microns meaning that they would not have been sampled. Nevertheless, the bias alone cannot explain the difference since it was reported by Subagyo *et al.*[5] that droplets of a diameter between 0.3 to 90 mm were observed. In this study, the maximum diameter was roughly 10 mm. By a visual verification, no droplets that exceeds the focal area could have been detected. Another evidence for a relation between the droplet size and the fluid properties can be derived from the critical Weber number at which droplets disintegrate into smaller ones. Koria and Lange[30] found critical Weber numbers in the range between 81 and 150 for raw iron. Using this value and the averaged droplet velocities of this study, the critical diameter at which water droplets are stable is about 3 mm. Using the same conditions, the critical diameter for raw iron is roughly three times from those of water. In fact, some larger droplets found in this study showed strong constriction in the middle of the major axis indicating the onset of disintegration as shown in **Figure 12**.

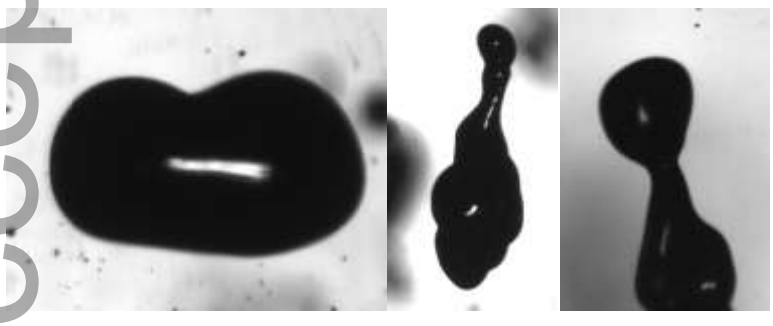

Figure 12: Disintegrating droplets

Since the depth of the focal area is not exactly known, it is not possible to derive a droplet generation rate from the sampled data. However, the number of detected droplets is directly correlated to the generation rate. The results of this study are very similar to those by Standish und He[26]. In accordance with this work, they found that the droplet generation rate increases with decreasing lance height up to a maximum at about 100 mm. Thereafter, the droplet

generation rate decrease, which was explained by the cavity transition from splashing to penetrating mode. This exact transition point, that might be of crucial important for prevention of splashing problems could not be determined experimentally due the coarse height adjustment of the top lance in this study, and remains a potential topic for further research.

The individual droplet properties measured directly in this study can be used to reconstruct individual droplet trajectories. **Figure 13** shows 100 exemplary droplets, recorded at the measurement position closest to the lance at a lance height of 100mm. The trajectories are computed using Eq. 14 to calculate the drag coefficient. Individual diameters, velocities and splashing angles were used for all trajectories. This data can be used to validate computational fluid dynamic models or to estimate the residual time of droplets, for example.

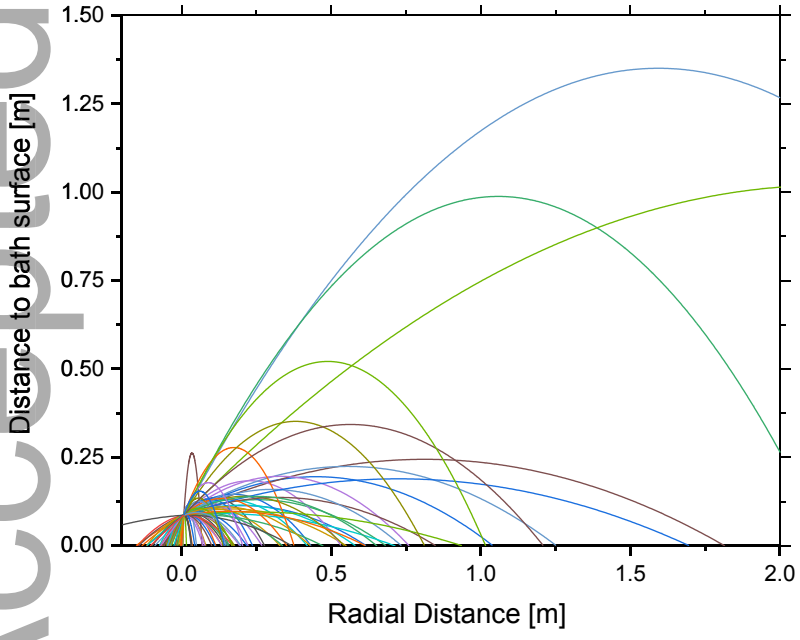

Figure 13: Reconstruction of individual trajectories for a lance height of 100 mm (N_B=5.92)

5. Conclusion

The experiments showed that existing diameter correlations are biased towards larger droplets and that they overfit the results yielded with molten metal. A more comprehensive correction should be based on measurements with different fluids covering a broad range of densities,

viscosities and surface tensions. By that, different processes or process stages with altering fluid properties can be modeled more accurate. This measurement should cover a broad range of measurement positions, as it was found that the droplet quantities strongly depend upon the sampling position. In addition, it was found that the relation between splashing angle and cavity mode is weaker than assumed in the literature. Further measurements with different nozzle inclination angles, nozzle diameters, fluid properties and additional lance heights are suggested to correlate average droplet trajectories with the blowing number. These studies should also yield a more comprehensive understanding about the splashing phenomenon and the exact point of cavity mode transition. As the droplet generation rate drops significantly at that point, it might be of crucial important for the optimization of lance head designs and blowing practices.

Acknowledgements

V.-V. Visuri thanks SYMMET research project for his funding during a research visit at RWTH Aachen University.

Received: ((will be filled in by the editorial staff))
Revised: ((will be filled in by the editorial staff))
Published online: ((will be filled in by the editorial staff))

References

[1] W. Kleppe, F. Oeters, *Archiv für das Eisenhüttenwesen*, **1976**. 47, 5,
[2] S.C. Koria, *Doktor-Ingenieur Thesis*, RWTH Aachen University **1981**
[3] S.C. Koria, K.W. Lange, *Metallurgical Transactions B*, **1984**. 15B,
[4] S.C. Koria, K.W. Lange, *Ironmaking and Steelmaking*, **1986**. 12, 5,
[5] Subagyo, G.A. Brooks, K.S. Coley, G.A. Irons, *ISIJ International*, **2003**. 43, 7,
[6] G. Brooks, Y. Pan, *Trans. B*, **2005**,
[7] N. Dogan, G. Brooks, M.A. Rhamdhani, *ISIJ international*, **2009**. 49, 1,
[8] M. Alam, G. Irons, G. Brooks, A. Fontana, J. Naser, *ISIJ International*, **2011**. 51, 9,
[9] S. Sabah, G. Brooks, *ISIJ international*, **2014**. 54, 4,
[10] S. Sabah, G. Brooks, *Metallurgical and Materials Transactions B*, **2015**. 46, 2,
[11] B.k. Rout, G. Brooks, Subagyo, M.A. Rhamdhani, Z. Li, *Metallurgical and Materials Transactions*, **2016**. 47B,

[12] F. Ji, M. Rhamdhani, M. Barati, K. Coley, G. Brooks, G. Irons, S. Nightingale, *High Temperature Materials and Processes*, **2003**. 22, 5-6,
[13] F.R. Block, A. Masui, G. Stolzenberg, *Archiv für das Eisenhüttenwesen*, **1973**. 44, 5,
[14] Q.L. He, N. Standish, *ISIJ International*, **1990**. 30, 4,
[15] R. Li, R. Harris, *Proc., IMM, London*, **1995**. 107,
[16] B. Deo, R. Boom, *Fundamentals of steelmaking metallurgy*, Prentice-Hall, **1993**.
[17] S.C. Koria, K.W. Lange, *Archiv für das Eisenhüttenwesen*, **1984**. 55, 12,
[18] G. Brooks, S. Sabah, B. Rout, Z. Li. *Splash Generation in Oxygen Steelmaking: What is Known?* **2017**. AISTech.
[19] V.-V. Visuri, M. Järvinen, A. Kärnä, P. Sulasalmi, E.-P. Heikkinen, P. Kupari, T. Fabritius, *Metallurgical and Materials Transactions B*, **2017**. 48, 3,
[20] B.K. Rout, G. Brooks, M.A. Rhamdhani, Z. Li, F.N. Schrama, A. Overbosch, *Metallurgical and Materials Transactions B*, **2018**. 49, 3,
[21] A. Kärnä, M. Järvinen, P. Sulasalmi, V.V. Visuri, S. Ollila, T. Fabritius, *steel research international*, **2018**. 89, 10,
[22] Q. Li, M. Li, S. Kuang, Z. Zou, *Metallurgical and Materials Transactions B*, **2015**. 46, 3,
[23] A. Nordquist, N. Kumbhat, L. Jonsson, P. Jönsson, *Steel Research International*, **2006**. 77, 2,
[24] N. Asahara, K.-i. Naito, I. Kitagawa, M. Matsuo, M. Kumakura, M. Iwasaki, *steel research international*, **2011**. 82, 5,
[25] K. Dong, R. Zhu, W. Gao, F.-h. Liu, *International Journal of Minerals, Metallurgy, and Materials*, **2014**. 21, 6,
[26] N. Standish, Q.L. He, *ISIJ International*, **1989**. 29, 6,
[27] M.J. Luomala, T.M.J. Fabritius, E.O. Virtanen, T.P. Siivola, T.L.J. Fabritius, H. Tenkku, auml, J.J. rkki, *ISIJ International*, **2002**. 42, 11,
[28] N.A. Molloy, *Jounal of The Iron and Steel Institute*, **1979**,
[29] R. Clift, J.R. Grace, M.E. Weber, *Bubbles, drops, and particles*, Courier Corporation, **2005**.
[30] S.C. Koria, K.W. Lange, *Canadian Metallurgical Quarterly*, **1979**. 18, 2,

A novel measurement technique is developed to analyze splashing droplets while top blowing in a water model. Simultaneously the droplet size, velocity, number and direction get recorded for different measurement positions and lance configurations. The results reveal a bias in existing correlations and yield splashing trajectories for different blowing numbers.